

## Hexagonal Growth of Ytterbium Nanoparticles by N<sub>2</sub> Gas Deposition

M. Jeřáb

Charles University, Faculty of Mathematics and Physics, Prague, Czech Republic.

K. Sakurai

National institute for material science, Tsukuba, Ibaraki, Japan.

**Abstract.** During last decade, nanotechnology has gained a significant relevance in many areas of basic research and applied science. One of the great challenges in the field of nanotechnology is preparation of nanoparticles and nanostructures where new, not ordinary materials are used. In the present study, we observed self organizing structures prepared by the gas deposition method in N<sub>2</sub> atmosphere. Glass palte served as a substrate. Typically, the structures have shape of hexagonal pyramid with base diagonal length higher then 2 μm. Characterization of the structures was performed utilizing Atomic Force Microscopy (AFM) and several X-ray techniques. The crystallographic structure determined by X-ray diffraction (XRD) corresponds to FCC ytterbium however signals corresponding to hexagonal ytterbium and YbN can be also observed. XRD pattern shows significantly more intense (111) diffraction peak which can be explained by the presence of hexagonal structures.

### Introduction

Nanotechnology plays an important role in various industrial applications. Study of nanostructures has become a significant issue not only in basic materials research but also in applied nanotechnology. The nanostructure materials have typically different physical and chemical properties than their micrometric equivalents. Recently, new and uncommon materials are investigated. Rare earth element nanoparticles are attractive due to their specific chemical and physical properties. One of the most interesting elements from lanthanide series is ytterbium (Yb) [Hampel, 1968]. Ytterbium serves mainly as dopant for variety of functional materials. Due to its unique electric properties, it is mainly used in active media for optics (lasers, solar cells) [Palik, 1991; Peters et al., 2002; Takaichi et al., 2004; Tokurakawa et al., 2006; Bisson et al., 2007].

Up to day, there is very few reports on the formation of Yb based nanostructures [Yada et al., 2002; Kuzmin et al., 2004a,b]. Successful synthesis of ytterbium nanoparticles by chemical routes was achieved only a few years ago [Ascencio et al., 2004]. Kuzmin et al. [2004a] reported growth of 3D ytterbium-silicide islands of nanometric size. In the present study, we have employed a completely different technique, the gas deposition method (also called gas evaporation technique), which is based on the vacuum deposition and it can be used for preparation of various kinds of fine metal particles [Bryant, 1971; Yatsuya et al., 1973; Kasukabe et al., 1974; Nishida and Kimoto, 1975; Ohno et al., 1976; Hayashi et al., 1977; Kaito, 1978; Starykov and Sakurai, 2005; Jerab and Sakurai, 2009].

Metallic ytterbium is evaporated by heating in a gas atmosphere. The particles are formed by solidification and aggregation during collisions with the gas molecules. The particles lose almost all their thermal kinetic energy during the collision. Based on this, the landing of the nanoparticles on the substrate is very soft and the nanoparticles do not transfer the energy to the substrate. Typically the inert gas (He, Ar) is used during gas deposition method. The reason for this is to prevent reaction of deposited material with working gas. The pure ytterbium

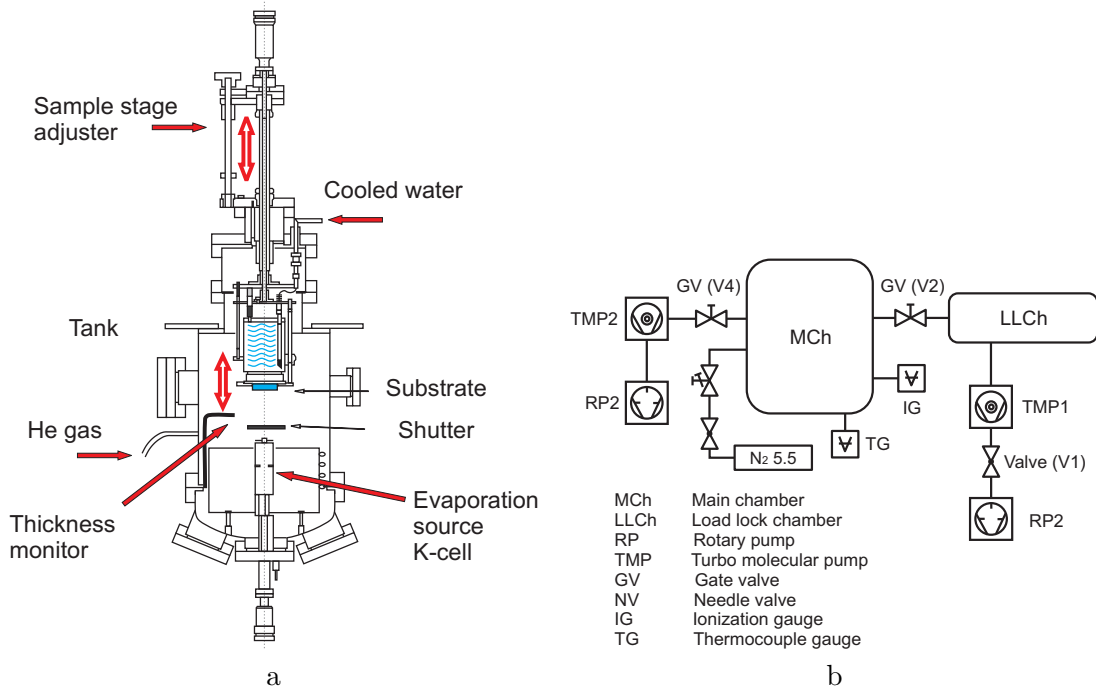


**Figure 1.** Illustrative schemes of the gas deposition apparatus. The apparatus is basically a vacuum evaporation chamber ( $10^{-6}$ – $10^{-7}$  Pa) equipped with a Knudsen evaporation cell (K-cell) and sample load lock system. The experiments can be switched from the ordinary vacuum evaporation to gas deposition simply by introducing the He gas. MCh: Main chamber, LLCh: Load lock chamber, RP: Rotary pump, TMP: Turbo molecular pump, GV: Gate valve, NV: Needle valve, IG: Ionization gauge, TG: Thermocouple gauge.

is very reactive metal and is very easily oxidized after exposing to normal atmosphere [Jerab and Sakurai, 2009]. In presented experiment  $N_2$  gas is used during the gas deposition. There is possibility to produce  $Yb_xN_{(1-x)}$  compound which is stable on air and have similar properties like pure Yb.

## Experiment

The apparatus used in the present experiment is basically a vacuum evaporation chamber equipped with a Knudsen evaporation cell (K-cell) and sample load lock system [Sarykov and Sakurai, 2005]. Minimal pressure achieved in the system is about  $10^{-6}$ – $10^{-7}$  Pa ( $10^{-8}$ – $10^{-9}$  Torr). The experiments can be switched from the ordinary vacuum evaporation to gas deposition simply by introducing the  $N_2$  gas. An illustrative scheme of the entire apparatus and components of the main chamber (MCh) is shown in Figure 1. The apparatus is composed of two separable chambers (main chamber MCh, load lock chamber LLCh) which are independently pumped by turbo molecular pumps. The load lock chamber with a linear motion of samples is separated from the main chamber by a gate valve. This set-up allows us to perform preparation of nanostructures in clean and well controlled conditions and prevents contamination of samples during deposition. The purity of used Ytterbium chips is 99.9% and that of used  $N_2$  gas of 99.99995%.

On the bottom of the main chamber is a K-cell with shutter from which the metallic ytterbium is evaporated by simple heating ( $500$ – $825$  °C, melting point is  $824$  °C) in the  $N_2$  environment ( $0.5$ – $25$  Pa). The evaporating temperature is controlled by a heating control unit with an accuracy of  $0.5$  °C. By this method, the nanoparticles are typically formed. Growing process is caused by solidification and aggregation of Yb atoms and particles during the collisions

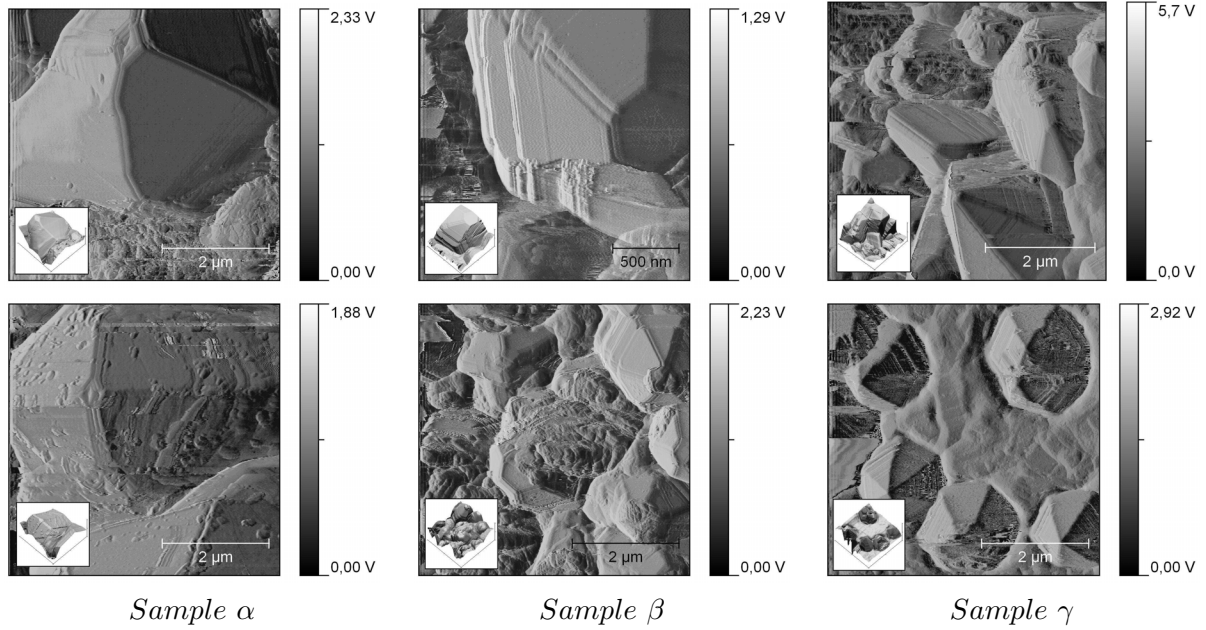


**Figure 2.** AFM deflection images of organized structures found on samples surfaces. These observations have been obtained on 3 samples prepared under following deposition conditions: temperature  $t_d = 500^\circ\text{C}$ , pressure  $P = 1\text{ Pa}$ , time  $t = 5\text{ hours}$  (Sample  $\alpha$ ); temperature  $t_d = 500^\circ\text{C}$ , pressure  $P = 1\text{ Pa}$ , time  $t = 3\text{ hours}$  (Sample  $\beta$ ) and temperature  $t_d = 400^\circ\text{C}$ , pressure  $P = 1\text{ Pa}$ , time  $t = 3\text{ hours}$  (Sample  $\gamma$ ); for all samples  $\text{N}_2$  working gas has been used. The roughness parameters of sample surface obtained by the AFM technique are:  $R_a = 532\text{ nm}$  and  $R_a = 558\text{ nm}$ ,  $R_{ms} = 642\text{ nm}$  and  $R_{ms} = 679\text{ nm}$  (Fig. 2a);  $R_a = 809\text{ nm}$  and  $R_a = 397\text{ nm}$ ,  $R_{ms} = 899\text{ nm}$  and  $R_{ms} = 482\text{ nm}$  (Fig. 2b);  $R_a = 1008\text{ nm}$  and  $R_a = 290\text{ nm}$ ,  $R_{ms} = 1105\text{ nm}$  and  $R_{ms} = 372\text{ nm}$  (Fig. 2c).

with  $\text{N}_2$  gas molecules. To collect floating particles, the glass substrate is placed close (10 mm) to the top of the K-cell. In order to eliminate further aggregation of deposited nanoparticles and their structure changes at the substrate surface caused by radiation heating, the back of the substrate is cooled by water. The deposition rate may be measured by a quartz thickness monitor.

The deposited thin film was analyzed using several different techniques. The surface roughness of samples was analyzed by processing of atomic force microscope (AFM) images (Shimadzu SPH-9500J3). X-ray reflectivity measurements (XRR) were applied to determine the thickness of the deposited film, as well as to estimate the surface and interface roughness. The crystal structure of the deposited film was studied by X-ray diffraction (XRD) and grazing incidence in plane X-ray diffraction (IPXRD). Rigaku PINT-ATX was used for all X-ray measurements.

## Experimental results

While ordinary gas deposition method produces Yb nanoparticles with typically spherical shape (size of the nanoparticles depends on deposition conditions—deposition temperature  $t_d$ , pressure of working gas  $P$ ) [Jerab and Sakurai, 2009], the hexagonal pyramid shaped structures were found to be present at the glass substrate surface. These observations have been obtained by AFM measurements on 3 samples ( $\alpha$ ,  $\beta$ ,  $\gamma$ ) depicted in Figure 2 prepared under deposition conditions: Sample  $\alpha$ : deposition temperature  $t_d = 500^\circ\text{C}$ , deposition pressure  $P = 1\text{ Pa}$ , deposition time  $t = 5\text{ hours}$ ; Sample  $\beta$ :  $t_d = 500^\circ\text{C}$ ,  $P = 1\text{ Pa}$ ,  $t = 3\text{ hours}$  and Sample  $\gamma$ :  $t_d = 400^\circ\text{C}$ ,  $P = 1\text{ Pa}$ ,  $t = 3\text{ hours}$ . For all samples, the  $\text{N}_2$  working gas has been used.

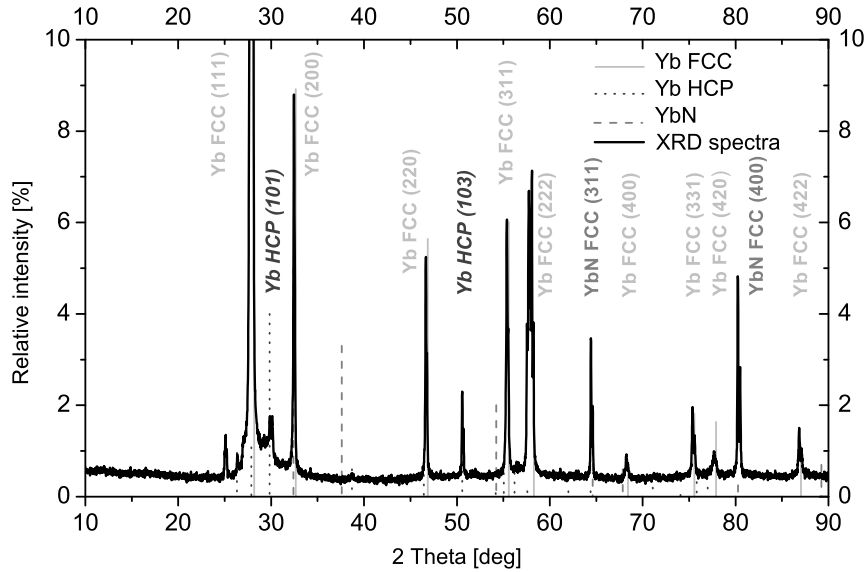


**Figure 3.** XRD measurement of Sample  $\beta$  ( $t_d = 500^\circ\text{C}$ ,  $P = 1$  Pa,  $t = 3$  hours). XRD data revealed deposited film has no single phase. In addition to FCC Yb metal, some HCP Yb metal and YbN diffraction peaks were observed.

### Crystallographic structure

X-Ray diffraction data (XRD) show that the main crystallographic structure of the deposited layers is the Yb FCC lattice—ytterbium beta allotropic form. However, peaks corresponding to hexagonal close packed (HCP) ytterbium lattice and YbN have been detected. In the Figure 3 the XRD pattern of the Sample  $\beta$  is shown. The data are normalized to the highest peak intensity corresponding to diffraction of Yb FCC (111) plane. The high of the peak was compared with the standard Yb powder XRD pattern. The intensity of (111) peak computed from the other measured peak intensities is approximately three times lower than measured (111) peak. Rest of the observed peaks of FCC Yb correspond to the powder FCC Yb XRD pattern. The results reveal that the preferred orientation of structures on the sample surface is (111). This fact brings important contribution to AFM images interpretation.

At  $\approx 30^\circ$  the peak of Yb HCP {101} plane diffraction can be found. The (103) plane diffraction peak attributed to Yb HCP diffraction pattern is around  $\approx 50^\circ$ . No other diffraction peaks of Yb HCP have been detected.

XRD measurements also revealed the presence of FCC YbN diffraction peaks (NaCl structure type—B1) corresponding to (311) and (400) planes. This may suggest that the evaporated Yb reacts with the  $\text{N}_2$  atmosphere during the deposition.

### Surface morphology and roughness

The sizes of observed structures differ from  $1.5\mu\text{m}$  up to  $5\mu\text{m}$ . The shape is typically hexagonal pyramid with smooth side planes although some structures of octahedron have been found (2). The roughness parameters of the samples obtained by the AFM measurement are  $R_a$  from 300 nm up to 1000 nm,  $R_{ms}$  380 nm up to 1100 nm, respectively. The roughness of the structures side planes is up to 100 nm (tables in Figures 4, 5, 6), though typical value is around 10 nm. This value corresponds to the roughness of spherical nanoparticles prepared by the same method and presented in Jerab and Sakurai [2009].

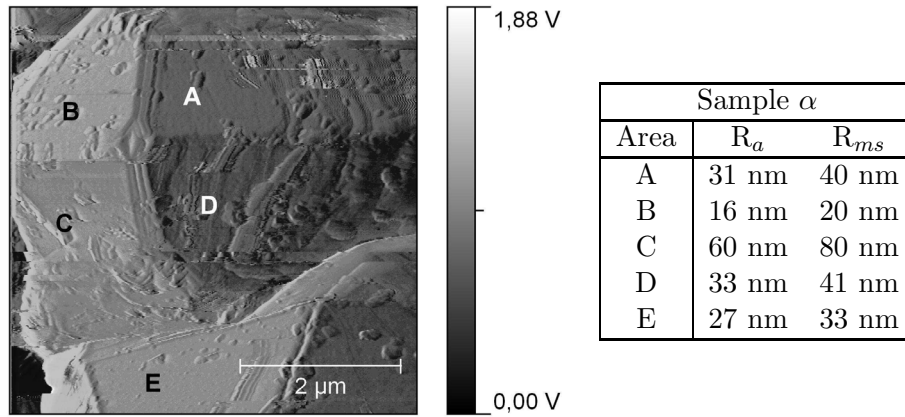


**Figure 4.** AFM image of studied hexagonal structure found on the Sample  $\alpha$  ( $t_d = 500^\circ\text{C}$ ,  $P = 1$  Pa,  $t = 5$  hours). The roughness of each side plane marked by a letter is computed from AFM high profile and shown in the table next to the AFM image.

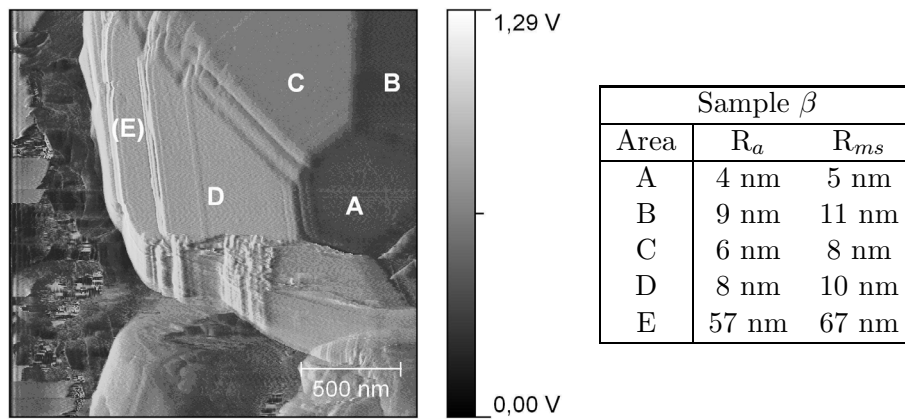


**Figure 5.** AFM image of studied hexagonal structure found on the Sample  $\beta$  ( $t_d = 500^\circ\text{C}$ ,  $P = 1$  Pa,  $t = 3$  hours). The roughness of each side plane marked by a letter is computed from AFM high profile and shown in the table next to the AFM image.

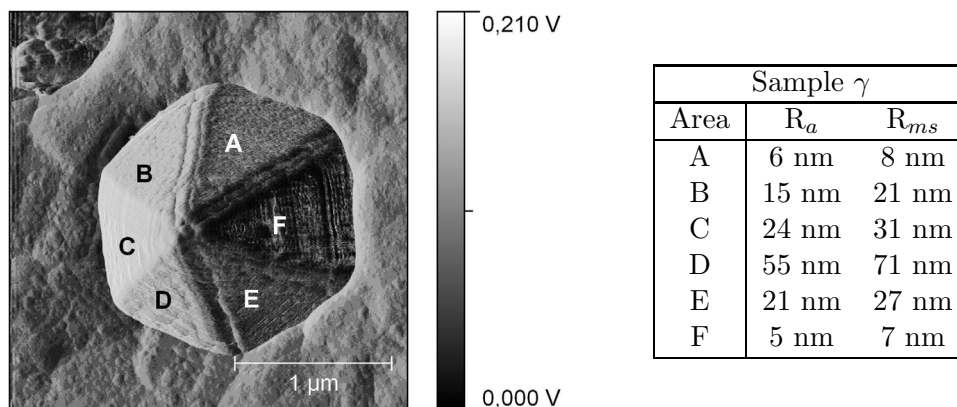


**Figure 6.** AFM image of studied hexagonal structure found on the Sample  $\gamma$  ( $t_d = 400^\circ\text{C}$ ,  $P = 1$  Pa,  $t = 3$  hours). The roughness of each side plane marked by a letter is computed from AFM high profile and shown in the table next to the AFM image.

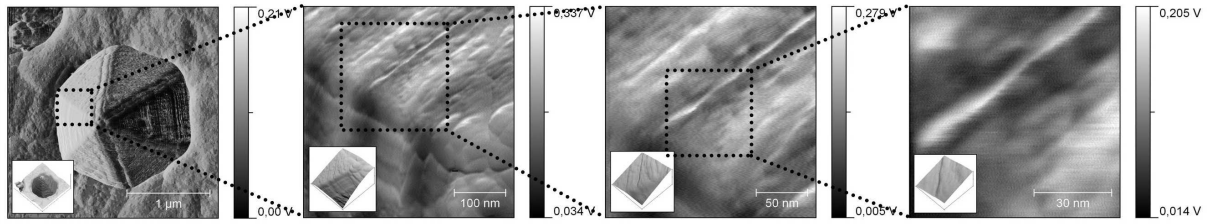


**Figure 7.** Sequence of magnified AFM deflection images of a hexagonal structure observed on the sample prepared under following conditions: deposition temperature  $t_d = 400^\circ\text{C}$ , deposition pressure  $P = 1\text{ Pa}$ , deposition time  $t = 3\text{ hours}$  – Sample C. For better visualization, the 3D images of the surface are shown.

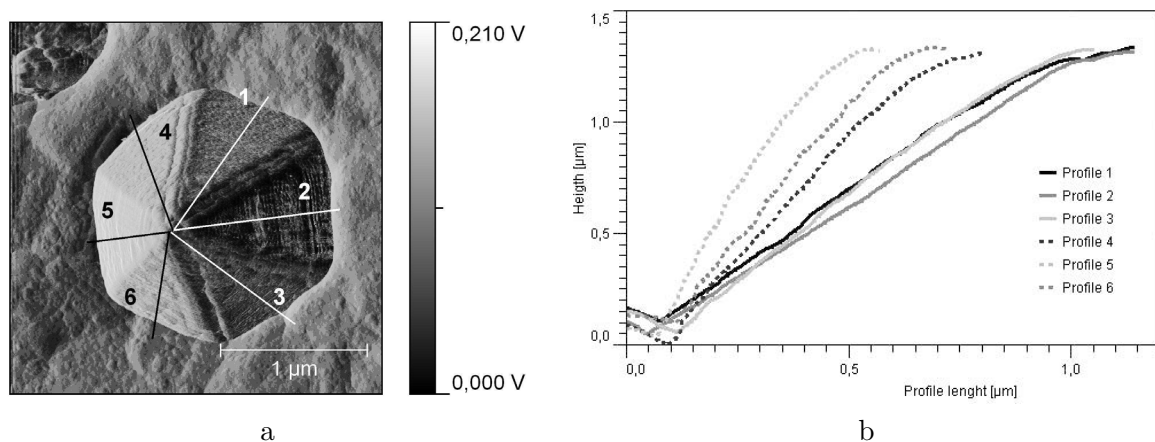
Figure 7 shows a sequence of magnified AFM images of observed hexagonal structure. One can see that the magnified areas have a stepped structure with a top view step distance of  $\approx 100\text{ nm}$ . The surface roughness of this areas is higher, around  $100\text{ nm}$ .

Figure 8 shows height profile of the hexagonal structure along depicted lines (lines 1–6) observed on sample  $\gamma$ . The height profiles exhibit a good linear increase from the heel of the structure to its top. Profiles 1–3 have similar slope angles around  $51^\circ$ . The slope angles of profiles 4–6 differ from previous one and their values are up to  $68^\circ$ .

The axis of symmetry of the observed structures is shifted from the perpendicular direction to the glass substrate (see 2). Some areas have the structures oriented in one direction (Figure 2c). We assume that this bent is caused by an angular distribution of deposition rate. However, Knudsen evaporation cell produce well homogenous profile of deposition rate, the sample is very close to the nozzle and even small inhomogeneity in deposition rate can be observed. It should be mentioned that all of the presented AFM images have been taken from central areas of the samples.

### Stability of hexagonal structures

In the Figure 9, the sequence of AFM deflection measurement is shown. The AFM images was obtained by contact mode measurement and deflection force  $\approx 1.6\text{ V}$  was applied (typically  $> 2\text{ V}$  is used). Scanning frequency  $0.5\text{ Hz}$  to line was also low (scanning time of one image  $\approx 17\text{ minutes}$ ). Although the silicate tip was used (Si is much softer material then Yb and



**Figure 8.** High profile of observed hexagonal structure. In Figure 8a, the traces of depicted profiles (8b) are show. The sample was prepared under conditions:  $t_d = 400^\circ\text{C}$ ,  $P = 1\text{ Pa}$ ,  $t = 3\text{ hours}$  – Sample  $\gamma$ .

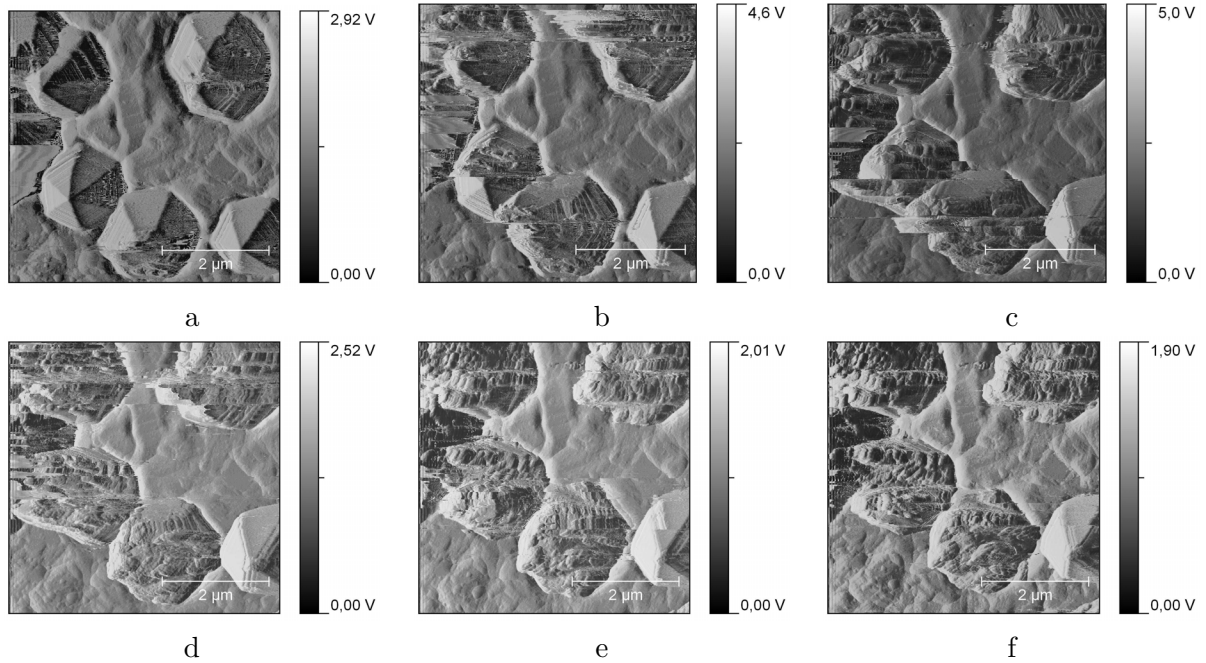


**Figure 9.** Sequence of AFM deflection images of organized structures found on sample surface prepared under deposition conditions: temperature  $t_d = 400^\circ\text{C}$ , pressure  $P = 1\text{ Pa}$ , time  $t = 3\text{ hours}$  – Sample  $\gamma$ . AFM images show that the hexagonal structures were easily destroyed during the AFM measurement even though the silicate tip was used and a small force was applied ( $\approx 1.6\text{ V}$ ).

scanning tip is typically blunted during measurement) and a small force was applied ( $\approx 1.6\text{ V}$ ), the hexagonal structures were easily destroyed during the AFM measurements. One can see that the hexagonal structure is systematically dismantled during the measurement by the scanning tip. After the destruction of hexagonal structures (Figures 9d-f), the sample is covered by the segments of underlying hexagonal structures. Roughness of this area becomes significantly higher ( $R_a = 0.116\ \mu\text{m}$ ,  $R_{ms} = 0.129\ \mu\text{m}$ ) then roughness of the side planes (compare with Figures 4 5, 6). Residual segments seams rounded with typical size  $\approx 0.14\ \mu\text{m}$ . This effect significantly limiting the quality of presented AFM images.

This fact may suggest that the observed structures are not ytterbium mono-crystals in a hexagonal shape, but they are probably some self-organized clusters of ytterbium nanoparticles in the hexagonal pyramid shape.

## Discussion and conclusion

During the preparation of ytterbium nanoparticles by the gas deposition method ( $\text{N}_2$  gas has been used), the organized structures were found to be present at the substrate surface. During the gas deposition technique some inert gas is typically used (e.g. He, Ar, Ne) to prevent the reaction of the deposited material with the working gas. In our experiment we used  $\text{N}_2$  gas instead of the inert gas. The reason for this was to produce ytterbium nitrides to prevent oxidation of ytterbium. We combined several different X-ray techniques and AFM measurements to characterize observed nanostructures.

The AFM images display that the structures are typically in a shape of hexagon pyramid with size of several micrometers ( $1.5\ \mu\text{m}$ – $5\ \mu\text{m}$ ). Hexagonal pyramids have generally very smooth side planes. Their roughness is around  $10\ \text{nm}$ , however could be up to  $100\ \text{nm}$ . The observed structures are typically symmetric but the axis of symmetry is shifted from perpendicular direction to substrate surface. This shift is caused by inhomogeneity of the deposition flux.

AFM images shows also that the observed structures are easily destroyed during the AFM measurement. This fact may suggest that the structures observed are not ytterbium mono-crystals, but these structures are probably some self-organized clusters of ytterbium nanoparticles in the hexagonal pyramid shape.

One can say that the morphology of the sample reflect the Yb HCP crystal lattice but XRD diffraction pattern of the sample shows that the crystallographic structure of deposited layer corresponds to Yb FCC lattice. In comparison with tabulated XRD pattern of Yb FCC powder the diffraction pattern of deposited layer exhibits approximately three times more intensive peak of (111) plane. This fact reveals that the deposited Yb growth takes place in preferred orientation of (111) plane. The growth of various FCC materials nanoparticles has been studied in many works [Kimoto and Nishida, 1967; Wada, 1968; Kasukabe et al., 1974; Ohno et al., 1976; Hayashi et al., 1977]. Hayashi et al. [1977] studied formation of ultrafine metal particles by gas-evaporation technique. This study was focused on FCC metal nanoparticles. Authors showed that (111) projection of octahedra nano-crystals seems like hexagons. Similar result presented [Wada, 1967], who showed presence of hexagonal plates on his sample. Their result connected with measured XRD results may explain the presence observed structures on samples surface.

XRD data show that during the deposition, the evaporated Yb may react with the N<sub>2</sub> atmosphere. This fact corresponds to presence of YbN revealed in the XRD measurement. Some peaks corresponding to the hexagonal ytterbium lattice can be found.

**Acknowledgments.** The work was done based on the collaboration program between the National Institute for Materials Science, Japan and Charles University, Czech Republic. The authors would like to thank Dr. M. Mizusawa for kind assistance during the research. The authors would also like to thank Mr. Penguin and A. Roguska for their great support during stay in Japan.

## References

- Ascencio, J. A., Rodríguez-Monroy, A. C., Liu, H. B., and Canizal, G., Synthesis and structure determination of ytterbium nanoparticles, *Chemistry Letters*, *33*, 1056–1057, 2004.
- Bisson, J. F., Kouznetsov, D., Ueda, K., Fredrich-Thornton, S. T., Petermann, K., and Huber, G., Switching of emissivity and photoconductivity in highly doped Yb<sup>3+</sup>:Y<sub>2</sub>O<sub>3</sub> and Lu<sub>2</sub>O<sub>3</sub> ceramics, *Applied Physics Letters*, *90*, 201901, URL <http://link.aip.org/link/?APL/90/201901/1>, 2007.
- Bryant, W. A., Vapor-phase formation of submicron ZrO<sub>2</sub>-coated chromium particles, *Journal of Vacuum Science and Technology*, *8*, 561–568, URL <http://link.aip.org/link/?JVS/8/561/1>, 1971.
- Hampel, C. A., ed., *The Encyclopedia of the Chemical Elements*, Reinhold Book Corporation, New York, USA, 1968.
- Hayashi, T., Ohno, T., Yatsuya, S., and Uyeda, R., Formation of ultrafine metal particles by gas-evaporation technique. IV. crystal habits of iron and FCC metals, Al, Co, Ni, Cu, Pd, Ag, In, Au and Pb, *Japanese Journal of Applied Physics*, *16*, 705–717, URL <http://jjap.ipap.jp/link?JJAP/16/705/>, 1977.
- Jerab, M. and Sakurai, K., X-ray analysis of Yb ultra thin film: Comparison of gas deposition and ordinary vacuum evaporation, *Adv. X-Ray Chem Anal. Jpn*, pp. 291–298, 2009.
- Kaito, C., Coalescence growth of smoke particles prepared by a gas-evaporation technique, *Japanese Journal of Applied Physics*, *17*, 601–609, URL <http://jjap.ipap.jp/link?JJAP/17/601/>, 1978.
- Kasukabe, S., Yatsuya, S., and Uyeda, R., Ultrafine metal particles formed by gas-evaporation technique. II. crystal habits of magnesium, manganese, beryllium and tellurium, *Japanese Journal of Applied Physics*, *13*, 1714–1721, URL <http://jjap.ipap.jp/link?JJAP/13/1714/>, 1974.
- Kimoto, K. and Nishida, I., An electron microscope and electron diffraction study of fine smoke particles prepared by evaporation in argon gas at low pressures (II), *Japanese Journal of Applied Physics*, *6*, 1047–1059, URL <http://jjap.ipap.jp/link?JJAP/6/1047/>, 1967.
- Kuzmin, M., Laukkanen, P., Perl, R. E., Vaara, R. L., and Vyyrynen, I. J., Formation of ytterbium silicide nanowires on Si(001), *Applied Surface Science*, *222*, 394–398, URL <http://dx.doi.org/10.1016/j.apsusc.2003.09.005>, 2004a.
- Kuzmin, M., Perl, R. E., Vaara, R. L., Laukkanen, P., and Vyyrynen, I. J., Formation of ytterbium silicide film on Si(001) by solid-phase epitaxy, *Journal of Crystal Growth*, *262*, 231–239, URL <http://dx.doi.org/10.1016/j.jcrysgro.2003.10.012>, 2004b.

- Nishida, I. and Kimoto, K., Electron microscope and electron diffraction study of fine particles prepared by evaporation in argon at low pressure. IV. fine particles of tellurium, *Japanese Journal of Applied Physics*, *14*, 1425–1432, URL <http://jjap.ipap.jp/link?JJAP/14/1425/>, 1975.
- Ohno, T., Yatsuya, S., and Uyeda, R., Formation of ultrafine metal particles by gas-evaporation technique. III. Al in He, Ar and Xe, and Mg in mixtures of inactive gas and air, *Japanese Journal of Applied Physics*, *15*, 1213–1217, URL <http://jjap.ipap.jp/link?JJAP/15/1213/>, 1976.
- Palik, E. D., ed., *Handbook of Optical Constants of Solids II*, Academic, New York, USA, pp. 1079, 1991.
- Peters, V., Bolz, A., Petermann, K., and Huber, G., Growth of high-melting sesquioxides by the heat exchanger method, *Journal of Crystal Growth*, *237–239*, 879–883, URL [http://dx.doi.org/10.1016/S0022-0248\(01\)02054-1](http://dx.doi.org/10.1016/S0022-0248(01)02054-1), 2002.
- Sarykov, O. and Sakurai, K., Determination of interface roughness of gd films deposited on si surface using improved wavelet transform of x-ray reflectivity data, *Applied Surface Science*, *244*, 235–239, URL [10.1016/j.apsusc.2004.10.124](http://dx.doi.org/10.1016/j.apsusc.2004.10.124), 12th International Conference on Solid Films and Surfaces, 2005.
- Takaichi, K., Yagi, H., Lu, J., Bisson, J., Shirakawa, A., Ueda, K., Yanagitani, T., and Kaminskii, A. A., Highly efficient continuous-wave operation at 1030 and 1075 nm wavelengths of ld-pumped  $\text{yb}^{3+}:\text{y}^{2+}_{203}$  ceramic lasers, *Applied Physics Letters*, *84*, 317–319, URL <http://dx.doi.org/10.1063/1.1641514>, 2004.
- Tokurakawa, M., Takaichi, K., Shirakawa, A., Ueda, K., Yagi, H., Hosokawa, S., Yanagitani, T., and Kaminskii, A. A., Diode-pumped mode-locked  $\text{yb}^{3+}:\text{lu}_2\text{o}_3$  ceramic laser, *Opt. Express*, *14*, 12832–12838, URL <http://dx.doi.org/10.1364/OE.14.012832>, 2006.
- Wada, N., Preparation of fine metal particles by means of evaporation in helium gas, *Japanese Journal of Applied Physics*, *6*, 553–556, URL <http://jjap.ipap.jp/link?JJAP/6/553/>, 1967.
- Wada, N., Preparation of fine metal particles by means of evaporation in xenon gas, *Japanese Journal of Applied Physics*, *7*, 1287–1293, URL <http://jjap.ipap.jp/link?JJAP/7/1287/>, 1968.
- Yada, M., Mihara, M., Mouri, S., Kuroki, M., and Kijima, T., Rare earth (Er, Tm, Yb, Lu) oxide nanotubes templated by dodecylsulfate assemblies, *Advanced Materials*, *14*, 309–313, URL [http://dx.doi.org/10.1002/1521-4095\(20020219\)14:4<309::AID-ADMA309>3.0.CO;2-Q](http://dx.doi.org/10.1002/1521-4095(20020219)14:4<309::AID-ADMA309>3.0.CO;2-Q), 2002.
- Yatsuya, S., Kasukabe, S., and Uyeda, R., Formation of ultrafine metal particles by gas evaporation technique. I. aluminium in helium, *Japanese Journal of Applied Physics*, *12*, 1675–1684, URL <http://jjap.ipap.jp/link?JJAP/12/1675/>, 1973.